Baroclinic transition in acoustic streaming: beyond Rayleigh's paradigm

Remil Mushthaq, Guillaume Michel, Gregory P Chini

J. Fluid Mech. (2025), *vol.* 1017, A32, doi:10.1017/jfm.2025.10450

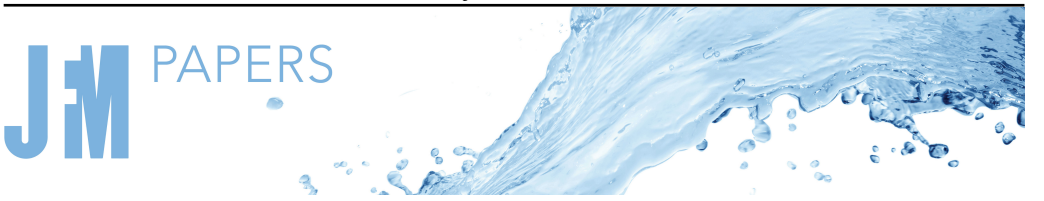

Baroclinic transition in acoustic streaming: beyond Rayleigh's paradigm

Remil Mushthaq[1], **Guillaume Michel**[2] **and Gregory P. Chini**[1,3]

[1]Department of Mechanical Engineering, University of New Hampshire, Durham, NH 03824, USA

[2]Sorbonne Université, CNRS, Institut Jean Le Rond d'Alembert, F-75005 Paris, France

[3]Program in Integrated Applied Mathematics, University of New Hampshire, Durham, NH 03824, USA

Corresponding author: Guillaume Michel, guillaume.michel@sorbonne-universite.fr

(Received 4 March 2025; revised 13 June 2025; accepted 6 July 2025)

Standing acoustic waves in a channel generate time-mean Eulerian flows. In homogeneous fluids, these streaming flows have been shown by Rayleigh to result from viscous attenuation of the waves in oscillatory boundary (i.e. Stokes) layers. However, the strength and structure of the mean flow significantly depart from the predictions of Rayleigh when inhomogeneities in fluid compressibility or density are present. This change in mean flow behaviour is of particular interest in thermal management, as streaming flows can be used to enhance cooling. In this work, we consider standing acoustic wave oscillations of an ideal gas in a differentially heated channel with hot- and cold-wall temperatures respectively set to $T_* + \Delta\Theta_*$ and T_*. An asymptotic analysis for a normalised temperature differential $\Delta\Theta_*/T_*$ comparable to the small acoustic Mach number is performed to capture the transition between the two documented regimes of Rayleigh streaming ($\Delta\Theta_* = 0$) and baroclinic streaming ($\Delta\Theta_* = O(T_*)$). Our analytical solution accounts for existing experimental and numerical results and elucidates the separate contributions of viscous torques in Stokes layers and baroclinic forcing in the interior to driving the streaming flow. The analysis yields a scaling estimate for the temperature difference $\Delta\Theta_{c_*}$ at which baroclinic driving is comparable to viscous forcing, signalling the smooth transition from Rayleigh to baroclinic acoustic streaming.

Key words: gas dynamics

1. Introduction

Since the seminal work of Rayleigh (1884, 1896), Eulerian time-mean flows generated by standing acoustic waves have garnered significant interest. As reviewed by Riley (1997,

2001), these streaming flows occur when the divergence of the wave-induced Reynolds stress cannot be fully balanced by a mean pressure gradient, i.e. when the waves have non-zero vorticity. In a channel filled with a homogeneous fluid, standing acoustic waves are irrotational in most of the domain, and streaming flows are driven by wave-induced viscous torques that arise in thin oscillatory boundary (i.e. Stokes) layers. The mean flows in this Rayleigh streaming regime have a characteristic speed $U_{s_*} = U_*^2/a_*$, where U_* is the typical value of the oscillating acoustic velocity and a_* the speed of sound, and are utilized predominantly in microfluidic applications (Bengtsson & Laurell 2004). The streaming flows driven by standing acoustic waves in an inhomogeneous fluid differ radically. Experiments conducted in thermally stratified gases reveal streaming patterns distinct from those predicted by Rayleigh and streaming velocities that are two orders of magnitude larger than U_*^2/a_* (Loh *et al.* 2002; Hyun, Lee & Loh 2005; Stockwald *et al.* 2014). These effects were also reported in direct numerical simulations (DNS) of the compressible Navier–Stokes equations (Lin & Farouk 2008; Aktas & Ozgumus 2010). To explain these features, a set of wave/mean-flow equations that captures the dynamics of streaming flows in strongly inhomogeneous gases was derived by Chini, Malecha & Dreeben (2014). In this framework, the temperature is assumed to vary significantly across the domain (specifically, the imposed temperature difference $\Delta\Theta_* = O(T_*)$, with T_* the cold-wall temperature), and the resulting streaming flows, of characteristic speed $U_{s_*} = U_*$, are found to be driven predominantly by the wave-induced Reynolds stress divergence in the bulk. Indeed, in inhomogeneous gases, acoustic waves acquire vorticity as a result of an inviscid process termed baroclinicity, and this regime is therefore referred to as 'baroclinic streaming'. Unlike Rayleigh streaming, baroclinic streaming is characterised by two-way coupling: the streaming flow driven by the waves modifies the temperature field, which in turn alters the structure of the waves. This approach can be extended to liquids, for which inhomogeneities in compressibility must also be included (Karlsen, Augustsson & Bruus 2016).

Acoustic streaming in straight channels with differentially heated walls has been extensively studied both numerically and experimentally to document this departure from Rayleigh streaming. Recent experiments of Qiu *et al.* (2021) demonstrate that inhomogeneities in liquid microchannels induced by thermal gradients can give rise to remarkably fast and distinctly patterned acoustic streaming. Their results underscore the critical role of baroclinic effects, even at modest temperature gradients. Here, we restrict our discussion to gases, for which significant density variations can be achieved. Large temperature differences have been treated experimentally (Hyun *et al.* 2005; Stockwald *et al.* 2014; Michel & Gissinger 2021) and numerically (Lin & Farouk 2008; Aktas & Ozgumus 2010), in which case the streaming flows can be analysed by assuming that $\Delta\Theta_* = O(T_*)$ (Michel & Chini 2019; Massih *et al.* 2024). However, experiments also demonstrate that Rayleigh streaming patterns are modified by temperature differences as small as a fraction of a degree (Nabavi, Siddiqui & Dargahi 2008). Although Rayleigh ($\Delta\Theta_* = 0$) and baroclinic ($\Delta\Theta_* = O(T_*)$) acoustic streaming have been separately studied extensively, an analytical solution bridging the transition between these regimes has not yet been reported in the more general setting when both processes are operative. Prior efforts to quantify the transition under the thin microchannel approximation ($k_* H_* \ll 1$) offer insight in a restricted regime (Daru *et al.* 2021).

In the present study, such a solution is derived for an ideal gas confined in a differentially heated straight channel and driven by a standing acoustic wave oscillating in the wall-parallel ('horizontal') direction. The aspect ratio of the set-up is $O(1)$, and buoyancy is neglected. A systematic asymptotic analysis enables the solution to be derived in the interior of the domain as well as in the oscillatory boundary layers (BLs).

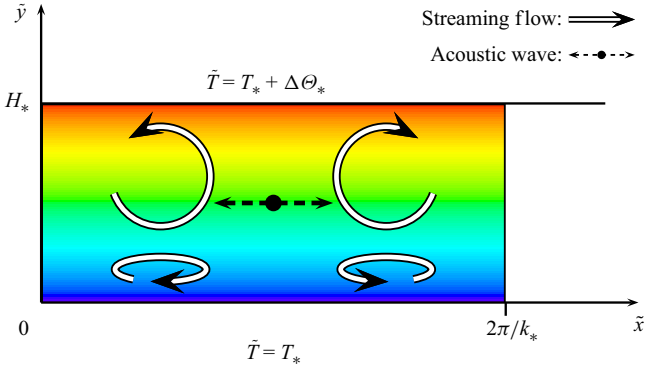

Figure 1. Schematic of the flow configuration. An ideal gas is confined between two horizontal, no-slip and impermeable walls separated by a distance H_*. The temperatures of the cold and hot walls are fixed at T_* and $T_* + \Delta\Theta_*$, respectively. Gravity is neglected. In the regime where the mean flow transitions from Rayleigh to baroclinic streaming, a standing acoustic wave of horizontal wavenumber k_* generates a counter-rotating stacked cellular streaming flow, where the cells closer to the hot wall span the majority of the channel height.

The contributions from viscous attenuation in the BLs and baroclinic forcing in the interior to driving the streaming flow are analysed in detail, and the critical temperature difference at which the flow transitions from Rayleigh to baroclinic streaming is determined as a function of the governing parameters. This result should provide useful guidance for future experimental and numerical studies by revealing whether one streaming mechanism dominates or both BL forcing and baroclinicity must be considered.

The remainder of this article is organised as follows. The two-time-scale wave/mean-flow system is introduced in § 2. The asymptotic analysis of and the explicit analytical solution to this system are presented in § 3. This solution is then validated against existing theoretical work, numerical results and experimental observations (§ 4). A summary of our key findings, which are contrasted with Rayleigh streaming and baroclinic acoustic streaming occurring in isolation, is given in § 5.

2. Problem formulation

2.1. *Flow configuration*

We investigate streaming of an ideal gas in a differentially heated horizontal channel subjected to standing horizontal acoustic-wave oscillations having a wavelength commensurate with the channel height, as illustrated in figure 1. Except for the temperature difference $\Delta\Theta_*$ that is assumed much smaller, this set-up is similar to that used to investigate baroclinic acoustic streaming in Massih *et al.* (2024). The dimensional variables and parameters, defined in table 1, are indicated using tildes and asterisks, respectively. Gravity is neglected and only two-dimensional dynamics is considered. Periodic boundary conditions are imposed along the horizontal ($\tilde{x}$) direction, setting the horizontal wavelength $2\pi/k_*$. The hot and cold walls are modelled as no-slip, no-penetration, isothermal boundaries maintained at constant but different temperatures, respectively $T_* + \Delta\Theta_*$ and T_*. In the absence of the acoustic wave, heat simply diffuses across the channel: there is no fluid motion, and the steady temperature profile is linear in the wall-normal ($\tilde{y}$) coordinate. A wall-parallel conservative acoustic body force of angular frequency ω_* excites and sustains the acoustic waves without directly driving a mean flow. The system is governed by the compressible Navier–Stokes equations,

Dimensional variable or parameter	Definition
$\tilde{\boldsymbol{u}} = (\tilde{u}, \tilde{v})$	Gas velocity
$\tilde{\rho}$	Gas density
$\tilde{p}$	Gas pressure
$\tilde{T}$	Gas temperature
$\tilde{\mathbb{F}}$	External force density
$(\tilde{x}, \tilde{y})$	Wall-parallel, wall-normal coordinates (referred to as horizontal and vertical, respectively)
$\tilde{t}$	Time variable
H_*	Channel height
$2\pi/k_*$	Horizontal wavelength of acoustic wave
μ_*	Dynamic viscosity
κ_*	Thermal conductivity
R_*	Specific gas constant
(c_{v_*}, c_{p_*})	Constant volume, pressure specific heat coefficient
$a_* = \sqrt{(c_{p_*}/c_{v_*})R_*T_*}$	Background sound speed
p_*	Background pressure
U_*	Typical acoustic wave velocity
u_{*max}	Maximum interior horizontal wave velocity

Table 1. Dimensional variables and parameters.

supplemented with conservation of mass and internal energy, and with the ideal gas equation of state:

$$\tilde{\rho}[\partial_{\tilde{t}}\tilde{\boldsymbol{u}} + (\tilde{\boldsymbol{u}} \cdot \tilde{\boldsymbol{\nabla}})\tilde{\boldsymbol{u}}] = -\tilde{\boldsymbol{\nabla}}\tilde{p} + \mu_* \left[\tilde{\boldsymbol{\nabla}}^2\tilde{\boldsymbol{u}} + \frac{1}{3}\tilde{\boldsymbol{\nabla}}(\tilde{\boldsymbol{\nabla}} \cdot \tilde{\boldsymbol{u}})\right] + \tilde{\mathbb{F}}(\tilde{x}, \tilde{t})\, \boldsymbol{e}_x, \tag{2.1}$$

$$\partial_{\tilde{t}}\tilde{\rho} + \tilde{\boldsymbol{\nabla}} \cdot (\tilde{\rho}\tilde{\boldsymbol{u}}) = 0, \tag{2.2}$$

$$\tilde{\rho} c_v [\partial_{\tilde{t}}\tilde{T} + (\tilde{\boldsymbol{u}} \cdot \tilde{\boldsymbol{\nabla}})\tilde{T}] = -\tilde{p}(\tilde{\boldsymbol{\nabla}} \cdot \tilde{u}) + \kappa_* \tilde{\nabla}^2 \tilde{T}, \tag{2.3}$$

$$\tilde{p} = \tilde{\rho} R_* \tilde{T}, \tag{2.4}$$

where $\tilde{\rho}$, $\tilde{p}$, $\tilde{T}$ and $\tilde{\boldsymbol{u}} = (\tilde{u}, \tilde{v})$ denote the density, pressure, temperature and velocity fields, respectively, and $\tilde{\boldsymbol{\nabla}} \equiv (\partial_{\tilde{x}}, \partial_{\tilde{y}})$. Bulk viscosity and viscous heating are neglected for convenience and analytical tractability, as is the temperature dependence of the viscosity and thermal conductivity (see the discussion in Michel & Chini (2019)).

2.2. *Scaling and non-dimensionalisation*

The scalings and the definition of dimensionless variables and parameters are reported in table 2. Except for the imposed temperature difference, these scalings are similar to those reported in Massih *et al.* (2024). The acoustic Mach number ϵ, which is also the inverse of the Strouhal number associated with the oscillatory flow, is assumed small and is used to order the subsequent asymptotic analysis. In this study, the dimensionless temperature differential is assumed to be finite but weak: $\hat{\Gamma} = O(\epsilon)$. As will become evident, this scaling enables the streaming flow generated by viscous torques in oscillatory BLs and that from baroclinic torques in the interior of the domain to arise at the same order in ϵ. The remaining parameters, including the aspect ratio δ, are taken to be $O(1)$.

Note that the Reynolds and Péclet numbers $Re = O(1)$ and $Pe = O(1)$ here compare the nonlinear terms with viscous and thermal diffusion in the body of the fluid. Note that other definitions of these coefficients can be found in the literature: a 'wave' Reynolds number (Re_w) based on the sound speed is sometimes introduced ($Re_w = \rho_* a_*/(k_*\mu_*) = Re/\epsilon$,

Variable	Scale	Parameter	Definition	Scaling
x	k_*^{-1}	Acoustic Mach number ϵ	U_*/a_*	$\epsilon \ll 1$
y	H_*	Aspect ratio δ	$k_* H_*$	$\delta = O(1)$
t	$(a_* k_*)^{-1}$	Temperature difference $\hat{\Gamma}$	$\Delta\Theta_*/T_*$	$\hat{\Gamma} = \epsilon\Gamma = O(\epsilon)$
u	a_*	Reynolds number Re	$\rho_* U_*/(k_*\mu_*)$	$Re = O(1)$
v	$(k_* H_*)a_*$	Péclet number Pe	$\rho_* c_{p_*} U_*/(k_*\kappa_*)$	$Pe = O(1)$
ρ	$\rho_* \equiv p_*/(R_* T_*)$	Prandtl number Pr	$\mu_* c_{p*}/\kappa_*$	$Pr = Pe/Re = O(1)$
Θ	T_*	Specific heat ratio γ	c_{p_*}/c_{v_*}	$\gamma = O(1)$
P	p_*	Acoustic wave amplitude $\mathbb{A}$	$\gamma\, u_{*_{max}}/U_*$	$\mathbb{A} = O(1)$
$\mathbb{F}$	$k_*\, p_*$			

Table 2. Dimensionless variables and parameters, similar to the previous analysis of Massih *et al.* (2024) except for the dimensionless temperature difference $\hat{\Gamma}$, which in the present work is asymptotically small.

here $Re_w \gg 1$), which compares unsteady inertia with net viscous forces and confirms that viscous terms do not affect the waves at leading order; or a streaming Reynolds number (Re_s) based on the appropriate velocity scale for the streaming flow $U_{s_*} = \epsilon^2 a_*$ ($Re_s = \rho_* \epsilon^2 a_*/(k_*\mu_*) = \epsilon Re$, here $Re_s \ll 1$), showing that nonlinear advection plays no part in the dynamics of the streaming flow in the regimes we investigate (Lighthill 1978). Using the scalings detailed in table 2, the dimensionless set of equations can be expressed as

$$\rho\,[\partial_t \boldsymbol{u} + (\boldsymbol{u}\cdot\boldsymbol{\nabla})\boldsymbol{u}] = -\frac{1}{\gamma}\boldsymbol{\nabla} p + \frac{\epsilon}{Re}\left[\boldsymbol{\nabla}^2\boldsymbol{u} + \frac{1}{3}\boldsymbol{\nabla}(\boldsymbol{\nabla}\cdot\boldsymbol{u})\right] + \mathbb{F}(x,t)\boldsymbol{e}_x, \tag{2.5}$$

$$\partial_t \rho + \boldsymbol{\nabla}\cdot(\rho\boldsymbol{u}) = 0, \tag{2.6}$$

$$\rho\,[\partial_t T + (\boldsymbol{u}\cdot\boldsymbol{\nabla})T] = (1-\gamma)\,p\,(\boldsymbol{\nabla}\cdot u) + \frac{\gamma\,\epsilon}{Pe}\nabla^2 T, \tag{2.7}$$

$$p = \rho T, \tag{2.8}$$

where dimensionless variables are not decorated with tildes, $\boldsymbol{\nabla} \equiv (\partial_x, \delta^{-1}\partial_y)$ and the velocity field $\boldsymbol{u} \equiv (u, \delta v)$. No-slip and no-penetration boundary conditions are complemented with the thermal boundary conditions $T(x, y=0, t) = 1$ and $T(x, y = 1, t) = 1 + \epsilon\Gamma$.

The scaling of the Reynolds number $Re = O(1)$, implying $Re_w = O(1/\epsilon)$, ensures that viscous forcing is negligible in the interior of the domain for the leading-order acoustic wave dynamics. However, these viscous forces drive oscillatory BLs of typical dimensional width $\delta_{s_*} = \sqrt{\mu_*/(\rho_*\omega_*)} = k_*^{-1}\sqrt{\epsilon/Re}$. The dynamics in these oscillatory BLs near the cold and hot walls, hereafter referred to as C-BL and H-BL, is captured by introducing rescaled wall-normal coordinates $\eta_c \equiv \epsilon^{-1/2} y$ and $\eta_h \equiv \epsilon^{-1/2}(1-y)$, respectively. In the analysis that follows, the rescaled wall-normal coordinates in both BLs are commonly represented using η without a subscript.

3. Asymptotic analysis

The steady streaming and oscillating fields are disentangled by introducing the time average $\overline{q}$ of any field $q(x, y, t)$ over an acoustic wave period. Fields therefore can be split into mean and fluctuation components:

$$q\,(x, y, t) = \overline{q}\,(x, y) + q'\,(x, y, t)\,, \tag{3.1}$$

where q' is the fluctuating component and $\overline{q'} = 0$. Further, each field is asymptotically expanded in one-half powers of ϵ as shown below:

$$(u, v) = \epsilon\,(u_1', 0) + \epsilon^{3/2}\big(u_{3/2}', v_{3/2}'\big) + \epsilon^2\left[\big(u_2', v_2'\big) + (\overline{u}_2, \overline{v}_2)\right] + O(\epsilon^{5/2}), \tag{3.2}$$

$$P = 1 + \epsilon\,\pi_1' + \epsilon^{3/2}\pi_{3/2}' + \epsilon^2\left[\pi_2' + \overline{\pi}_2\right] + \epsilon^{5/2}\left[\pi_{5/2}' + \overline{\pi}_{5/2}\right] + \epsilon^3\left[\pi_3' + \overline{\pi}_3\right] + O(\epsilon^{7/2}), \tag{3.3}$$

$$\Theta = 1 + \epsilon\,\left[\Gamma\, y + \Theta_1'\right] + \epsilon^{3/2}\Theta_{3/2}' + \epsilon^2\left[\overline{\Theta}_2 + \Theta_2'\right] + O(\epsilon^{5/2}), \tag{3.4}$$

$$\rho = 1 + \epsilon\,\left[\overline{\rho}_1 + \rho_1'\right] + \epsilon^{3/2}\rho_{3/2}' + \epsilon^2\left[\overline{\rho}_2 + \rho_2'\right] + O(\epsilon^{5/2}), \tag{3.5}$$

$$\mathbb{F} = \epsilon^{3/2}\mathbb{F}_{3/2}'(x, t) + O(\epsilon^2). \tag{3.6}$$

Here, we consider a plane horizontal standing acoustic wave of $O(\epsilon)$ amplitude. Note that expansion in fractional powers of ϵ results from the existence of thin BLs of dimensionless width $O(\sqrt{\epsilon})$. Since, by construction, the leading-order wave fields are $O(\epsilon)$, the corrections are even smaller (i.e. approach zero faster than $O(\epsilon)$), and no $O(\sqrt{\epsilon})$ corrections to the mean fields are forced. The external force that sustains waves of wavenumber k_* and inverse angular frequency $(a_* k_*)^{-1}$, respectively used as the scales for x and t, is chosen to be of the form

$$\mathbb{F}_{3/2}'(x, t) = \mathbb{F}_{3/2}\sin(x)\,\mathrm{e}^{\mathrm{i}t} + \text{c.c.}, \tag{3.7}$$

where c.c. denotes the complex conjugate. An explicit analytical expression for the coefficient $\mathbb{F}_{3/2}$ is derived in § 3.5. The expansions for the various fields are then substituted into the dimensionless governing equations, and the dynamics at sequential orders in the small parameter ϵ is independently analysed.

3.1. *Acoustic and steady dynamics at* $O(1)$

At this order the gas is steady (all fluctuating and mean flow speeds are smaller than the speed of sound) and homogeneous (the imposed temperature difference is assumed to be small compared with the cold-wall temperature).

3.2. *Steady dynamics at* $O(\epsilon)$

No streaming flow arises at this order. The imposed temperature difference between the boundaries maintains the linear temperature and density profiles $\epsilon\Gamma y$ and $\epsilon\overline{\rho}_1$, with $\overline{\rho}_1 = -\Gamma y$.

3.3. *Acoustic dynamics at* $O(\epsilon)$

The $O(\epsilon)$ dynamics in the interior satisfies

$$\partial_t u_1' + \gamma^{-1}\partial_x \pi_1' = 0, \tag{3.8}$$

$$\partial_y \pi_1' = 0, \tag{3.9}$$

$$\partial_t \rho_1' + \partial_x u_1' = 0, \tag{3.10}$$

$$\partial_t \Theta_1' + (\gamma - 1)\,\partial_x u_1' = 0, \tag{3.11}$$

$$\pi_1' - \rho_1' - \Theta_1' = 0, \tag{3.12}$$

which can be collapsed to the one-dimensional second-order wave equation:

$$\partial_{tt}\pi_1' = \partial_{xx}\pi_1', \quad \text{with} \quad \partial_t u_1' = -\gamma^{-1}\partial_x \pi_1', \quad \rho_1' = \gamma^{-1}\pi_1', \quad \Theta_1' = (1-\gamma^{-1})\pi_1'. \tag{3.13}$$

Since the oscillatory flow driven by the plane wave does not satisfy the no-slip and isothermal boundary conditions at the walls, Stokes layers are generated.

The $O(\epsilon)$ dynamics in the BLs is governed by

$$\partial_t u_1' + \gamma^{-1}\partial_x \pi_1' - (Re\delta^2)^{-1}\partial_{\eta\eta} u_1' = 0, \tag{3.14}$$

$$\partial_\eta \pi_1' = 0, \tag{3.15}$$

$$\partial_t \rho_1' + \partial_x u_1' \pm \partial_\eta v_{3/2}' = 0, \tag{3.16}$$

$$\partial_t \Theta_1' + (\gamma-1)\,(\partial_x u_1' \pm \partial_\eta v_{3/2}') - \gamma (Pe\delta^2)^{-1}\partial_{\eta\eta}\Theta_1' = 0, \tag{3.17}$$

$$\pi_1' - \rho_1' - \Theta_1' = 0, \tag{3.18}$$

where the first-order wall-normal partial derivatives in the C-BL are $+\partial_\eta$ and those in the H-BL are $-\partial_\eta$.

The complete acoustic wave solution at $O(\epsilon)$, which satisfies the isothermal, no-slip and no-penetration conditions at the boundaries and asymptotically matches with the horizontal standing-wave solution obtained in the interior, is found to be

$$\pi_1' = \frac{\mathbb{A}}{2}\cos(x)\,\mathrm{e}^{\mathrm{i}t} + \text{c.c.} \qquad \text{(interior and BLs)}, \tag{3.19}$$

$$u_1' = \begin{cases} -\mathrm{i}\dfrac{\mathbb{A}}{2\gamma}\sin(x)\,\mathrm{e}^{\mathrm{i}t} + \text{c.c.} & \text{(interior)} \\ -\mathrm{i}\dfrac{\mathbb{A}}{2\gamma}(1-\mathrm{e}^{-(1+\mathrm{i})\sqrt{\mathbb{R}}\eta})\sin(x)\mathrm{e}^{\mathrm{i}t} + \text{c.c.} & \text{(BLs)}, \end{cases} \tag{3.20}$$

$$v_{3/2}' = \begin{cases} -\dfrac{\mathbb{A}(1+\mathrm{i})\,\cos(x)\mathrm{e}^{\mathrm{i}t}}{4\gamma\sqrt{\mathbb{R}\mathbb{P}}}[(1-\mathrm{e}^{-(1+\mathrm{i})\sqrt{\mathbb{R}}\eta})\sqrt{\mathbb{P}} + (\gamma-1)(1-\mathrm{e}^{-(1+\mathrm{i})\sqrt{\mathbb{P}}\eta})\sqrt{\mathbb{R}}] \\ \quad +\text{c.c.} \quad \text{(C-BL)} \\ \dfrac{\mathbb{A}(1+\mathrm{i})\,\cos(x)\mathrm{e}^{\mathrm{i}t}}{4\gamma\sqrt{\mathbb{R}\mathbb{P}}}[(1-\mathrm{e}^{-(1+\mathrm{i})\sqrt{\mathbb{R}}\eta})\sqrt{\mathbb{P}} + (\gamma-1)(1-\mathrm{e}^{-(1+\mathrm{i})\sqrt{\mathbb{P}}\eta})\sqrt{\mathbb{R}}] \\ \quad +\text{c.c.} \quad \text{(H-BL)}, \end{cases} \tag{3.21}$$

$$\Theta_1' = \begin{cases} (1-\gamma^{-1})\pi_1' & \text{(interior)} \\ (1-\gamma^{-1})\dfrac{\mathbb{A}}{2}(1-\mathrm{e}^{-(1+\mathrm{i})\sqrt{\mathbb{P}}\eta})\cos(x)\mathrm{e}^{\mathrm{i}t} + \text{c.c.} & \text{(BLs)}, \end{cases} \tag{3.22}$$

$$\rho_1' = \begin{cases} \gamma^{-1}\pi_1' & \text{(interior)} \\ \gamma^{-1}\dfrac{\mathbb{A}}{2}(1+(\gamma-1)\mathrm{e}^{-(1+\mathrm{i})\sqrt{\mathbb{P}}\eta})\cos(x)\mathrm{e}^{\mathrm{i}t} + \text{c.c.} & \text{(BLs)}. \end{cases} \tag{3.23}$$

Here, $\mathbb{R} \equiv Re\delta^2/2$ and $\mathbb{P} \equiv Pe\delta^2/2$ are the aspect-ratio-dependent Reynolds and Péclet numbers and $\mathbb{A}$ is the $O(1)$ acoustic pressure wave amplitude. The expression for $v_{3/2}'$ in the interior is derived in the higher-order analysis that follows. At $O(\epsilon)$, the acoustic velocity field in the interior is irrotational, and acoustic wave vorticity is confined to the BLs.

3.4. *Steady dynamics at* $O(\epsilon^{3/2})$

No corrections to the streaming fields arise at this order.

3.5. *Acoustic dynamics at* $O(\epsilon^{3/2})$

The vertical velocity that emerges in the leading-order BLs does not vanish as $\eta \to \infty$; see (3.21). The oscillating field it generates would, in the absence of forcing, lead to a slow decay of the leading-order wave amplitude. Here, a stationary state is sustained by the weak external forcing $\mathbb{F}'_{3/2}$ in the interior.

The governing equations at $O(\epsilon^{3/2})$ in the interior are

$$\partial_t u'_{3/2} + \gamma^{-1}\partial_x \pi'_{3/2} = \mathbb{F}_{3/2} \sin(x)\, \mathrm{e}^{\mathrm{i}t} + \text{c.c.}, \tag{3.24}$$

$$\partial_t v'_{3/2} + (\gamma\delta^2)^{-1}\partial_y \pi'_{3/2} = 0, \tag{3.25}$$

$$\partial_t \rho'_{3/2} + \partial_x u'_{3/2} + \partial_y v'_{3/2} = 0, \tag{3.26}$$

$$\partial_t \Theta'_{3/2} + (\gamma - 1)(\partial_x u'_{3/2} + \partial_y v'_{3/2}) = 0, \tag{3.27}$$

$$\pi'_{3/2} - \rho'_{3/2} - \Theta'_{3/2} = 0. \tag{3.28}$$

In the BLs the waves must satisfy

$$\partial_t u'_{3/2} + \gamma^{-1}\partial_x \pi'_{3/2} - (Re\delta^2)^{-1}\partial_{\eta\eta} u'_{3/2} = \mathbb{F}_{3/2} \sin(x)\, \mathrm{e}^{\mathrm{i}t} + \text{c.c.}, \tag{3.29}$$

$$\partial_\eta \pi'_{3/2} = 0, \tag{3.30}$$

$$\partial_t \rho'_{3/2} + \partial_x u'_{3/2} \pm \partial_\eta v'_2 = 0, \tag{3.31}$$

$$\partial_t \Theta'_{3/2} + (\gamma - 1)(\partial_x u'_{3/2} \pm \partial_\eta v'_2) - \gamma(Pe\delta^2)^{-1}\partial_{\eta\eta}\Theta'_{3/2} = 0, \tag{3.32}$$

$$\pi'_{3/2} - \rho'_{3/2} - \Theta'_{3/2} = 0. \tag{3.33}$$

This set of equations can be solved analytically with appropriate boundary and matching conditions; see Appendix A. In particular, the balance between external forcing and diffusion is explicit:

$$\mathbb{F}_{3/2} = (1 - i)\,\frac{\mathbb{A}}{2\,\gamma}\left(\frac{(\gamma - 1)}{\sqrt{\mathbb{P}}} + \frac{1}{\sqrt{\mathbb{R}}}\right). \tag{3.34}$$

At $O(\epsilon^{3/2})$, acoustic wave vorticity remains localised in the BLs ($\boldsymbol{\Omega}'_{3/2} = \boldsymbol{\nabla} \times \boldsymbol{u}'_{3/2} = \boldsymbol{0}$ in the interior, as shown by taking the curl of the momentum equations (3.24)–(3.25)).

3.6. *Steady dynamics at* $O(\epsilon^2)$ *(part 1)*

The $O(\epsilon^2)$ equations characterising the steady pressure field $\overline{\pi}_2$ in the interior are

$$\gamma^{-1}\partial_x \overline{\pi}_2 = -\overline{\rho'_1 \partial_t u'_1} - \overline{u'_1 \partial_x u'_1} = \overline{(\partial_t \rho'_1) u'_1} - \overline{u'_1 \partial_x u'_1} = -\partial_x \overline{(u'_1)^2}, \tag{3.35}$$

$$\partial_y \overline{\pi}_2 = 0, \tag{3.36}$$

where (3.35) has been simplified using (3.10). Thus, to within an arbitrary constant, the mean pressure $\overline{\pi}_2 = -\gamma\overline{(u'_1)^2}$.

A streaming flow emerges as the consequence of nonlinearity. Specifically, in the BLs,

$$(\boldsymbol{u}' \cdot \boldsymbol{\nabla})\boldsymbol{u}' = \boldsymbol{\nabla}\left(\frac{1}{2}\,\boldsymbol{u}' \cdot \boldsymbol{u}'\right) + (\boldsymbol{\nabla} \times \boldsymbol{u}') \times \boldsymbol{u}' \tag{3.37}$$

includes an $O(\epsilon^2)$ component $(\boldsymbol{\nabla} \times \boldsymbol{u}') \times \boldsymbol{u}'$ that (i) is non-zero since the $O(\epsilon)$ acoustic vorticity is non-zero in the BL, (ii) cannot be completely balanced by a pressure gradient

and (iii) consists of both an oscillating term proportional to e^{2it} that generates harmonics and, crucially, a steady component. As first established by Rayleigh, this term drives a streaming flow in the BL that is viscously communicated to the interior and that can be computed through the momentum equations only. The inertial term in the x-momentum equation can be transformed using (3.16) and recast as

$$\rho_1'\partial_t u_1' + u_1'\partial_x u_1' \pm v_{3/2}'\partial_\eta u_1' = \partial_t(\rho_1' u_1') + \partial_x\left(u_1'^2\right) \pm \partial_\eta\left(u_1' v_{3/2}'\right), \tag{3.38}$$

and we therefore consider

$$-\gamma^{-1}\partial_x\overline{\pi}_2 + (Re\delta^2)^{-1}\partial_{\eta\eta}\overline{u}_2 = \partial_x(\overline{u_1' u_1'}) \pm \partial_\eta(\overline{u_1' v_{3/2}'}), \tag{3.39}$$

$$\partial_\eta\overline{\pi}_2 = 0. \tag{3.40}$$

This reduced set of equations is unaltered by the imposed temperature difference and can be solved explicitly for $\overline{u}_2$ given the acoustic fields already derived, the expression for $\overline{\pi}_2$ in the interior and the boundary and matching conditions $\overline{u}_2(x, 0) = 0$ and $\lim_{\eta\to\infty}\partial_\eta\overline{u}_2(x, \eta) = 0$. The full solution is reported in Appendix B and has a non-zero limit as $\eta \to \infty$ that corresponds to an effective slip velocity $\overline{u}_{slip}$ acting on the interior flow, which is independent of the aspect ratio δ and given by

$$\overline{u}_{slip} = -\frac{3\mathbb{A}^2}{8\gamma^2(Pe + Re)}\left(Pe + \frac{2(\gamma-1)}{3}\sqrt{PeRe} + Re\right)\sin(2x). \tag{3.41}$$

Since $\gamma > 1$, the slip velocity is directed towards the acoustic wave velocity nodes (located at $x = p\pi$, $p \in \mathbb{Z}$) (Lighthill 1978). Its dimensional expression in the absence of thermal diffusivity is more commonly reported: setting $Pe \to \infty$ results in a dimensional slip velocity $\overline{u}_{slip_*} = -[3U_0^2/(8a_*)]\sin(2k_*\tilde{x})$, with $U_0 = (\mathbb{A}/\gamma)\epsilon a_*$ the amplitude of the leading-order acoustic wave velocity in the interior.

The streaming velocity field $\overline{\boldsymbol{u}}_2$ in the interior is found by solving the time-averaged momentum equation at $O(\epsilon^3)$ and the continuity equation at $O(\epsilon^2)$:

$$-\frac{\boldsymbol{\nabla}\overline{\pi}_3}{\gamma} + \frac{\boldsymbol{\nabla}^2\overline{\boldsymbol{u}}_2}{Re} = \overline{(\boldsymbol{u}_1'\cdot\boldsymbol{\nabla})\boldsymbol{u}_2' + (\boldsymbol{u}_{3/2}'\cdot\boldsymbol{\nabla})\boldsymbol{u}_{3/2}' + (\boldsymbol{u}_2'\cdot\boldsymbol{\nabla})\boldsymbol{u}_1' + \overline{\rho}_1(\boldsymbol{u}_1'\cdot\boldsymbol{\nabla})\boldsymbol{u}_1'} \\ \overline{+\rho_1'\partial_t\boldsymbol{u}_2' + \rho_{3/2}'\partial_t\boldsymbol{u}_{3/2}' + \rho_2'\partial_t\boldsymbol{u}_1'}, \tag{3.42}$$

$$\boldsymbol{\nabla}\cdot\overline{\boldsymbol{u}}_2 = 0, \tag{3.43}$$

where the nonlinear term $\partial_x(\overline{\rho_1' u_1'})$ has not been included in (3.43) because $\overline{\rho_1' u_1'} = 0$. Most of the nonlinear terms in (3.42) can be balanced by a pressure gradient and those driving streaming flows are readily identified by taking the curl of this equation. Since acoustic vorticity vanishes in the interior at $O(\epsilon)$ and $O(\epsilon^{3/2})$, substantial simplifications occur, detailed in Appendix C.1. With $\overline{\boldsymbol{u}}_2 = -\boldsymbol{\nabla}\times(\overline{\psi}_2\boldsymbol{e}_z)$ (i.e. $(\overline{u}_2, \overline{v}_2) = \delta^{-1}(-\partial_y\overline{\psi}_2, \partial_x\overline{\psi}_2)$), where $\boldsymbol{e}_z \equiv \boldsymbol{e}_x \times \boldsymbol{e}_y$, the stream function $\overline{\psi}_2$ can be obtained by solving the following equation:

$$\frac{1}{Re}\boldsymbol{\nabla}^4\overline{\psi}_2\boldsymbol{e}_z = \overline{\boldsymbol{\nabla}\times\left(\boldsymbol{\Omega}_2'\times\boldsymbol{u}_1'\right) + (\boldsymbol{\nabla}\overline{\rho}_1/2)\times\left[\boldsymbol{\nabla}\left(\boldsymbol{u}_1'\cdot\boldsymbol{u}_1'\right)\right] + \boldsymbol{u}_{3/2}'\times(\partial_t\mathbb{F}_{3/2}'\boldsymbol{e}_x)} \\ \overline{+\boldsymbol{\nabla}\times\left[\rho_1'\partial_t\boldsymbol{u}_2' + \rho_2'\partial_t\boldsymbol{u}_1'\right]}. \tag{3.44}$$

The $O(\epsilon^2)$ acoustic fields are required to proceed.

3.7. *Acoustic dynamics at $O(\epsilon^2)$*

The momentum equations governing the $O(\epsilon^2)$ acoustic dynamics in the interior are

$$\partial_t u_2' + \gamma^{-1}\partial_x \pi_2' = \left(\Gamma y - \rho_1'\right)\partial_t u_1' + \overline{\rho_1'\partial_t u_1'} - u_1'\partial_x u_1' + \overline{u_1'\partial_x u_1'} + (3Re)^{-1}4\partial_{xx}u_1' + \mathbb{F}_2(x,t), \tag{3.45}$$

$$\partial_t v_2' + (\gamma\delta^2)^{-1}\partial_y \pi_2' = 0, \tag{3.46}$$

$$\partial_t \rho_2' + \partial_x u_2' + \partial_y v_2' = -\partial_x\left[\left(\rho_1' - \Gamma y\right)u_1'\right] + \overline{\partial_x\left(\rho_1' u_1'\right)}, \tag{3.47}$$

$$\partial_t \Theta_2' + (\gamma - 1)\left(\partial_x u_2' + \partial_y v_2'\right) = \left(\Gamma y - \rho_1'\right)\partial_t\Theta_1' + \overline{\rho_1'\partial_t\Theta_1'} - u_1'\partial_x\Theta_1' + \overline{u_1'\partial_x\Theta_1'} + \gamma Pe^{-1}\partial_{xx}\Theta_1' + (1-\gamma)\left(\pi_1'\partial_x u_1' - \overline{\pi_1'\partial_x u_1'}\right), \tag{3.48}$$

$$\pi_2' - \rho_2' - \Theta_2' = \left(\Theta_1' + \Gamma y\right)\rho_1' - \overline{\Theta_1'\rho_1'} - \Gamma y\Theta_1'. \tag{3.49}$$

Since the leading-order acoustic fields in the interior do not depend on y, using (3.45) and (3.46) it can be seen that acoustic wave vorticity $\Omega_2' = \delta\partial_x v_2' - \delta^{-1}\partial_y u_2'$ is generated according to

$$\partial_t \Omega_2' = -\delta^{-1}\partial_y\left(\Gamma y\partial_t u_1'\right) = -\delta^{-1}\Gamma\partial_t u_1' \rightarrow \boldsymbol{\Omega}_2' = -\frac{\Gamma u_1'}{\delta}\boldsymbol{e}_z. \tag{3.50}$$

In contrast to corresponding results at $O(\epsilon)$ and $O(\epsilon^{3/2})$, at $O(\epsilon^2)$ the wave vorticity is non-zero as a result of the imposed temperature difference Γ. This solution can be used to evaluate certain nonlinear forcing terms already introduced, e.g.

$$\overline{(\nabla\overline{\rho}_1/2)\times\left[\nabla\left(\boldsymbol{u}_1'\cdot\boldsymbol{u}_1'\right)\right] + \nabla\times\left(\boldsymbol{\Omega}_2'\times\boldsymbol{u}_1'\right)} = -\overline{\left(\partial_x u_1'\right)\boldsymbol{\Omega}_2'} + \overline{\partial_x\left(u_1'\boldsymbol{\Omega}_2'\right)} = \overline{u_1'\partial_x\boldsymbol{\Omega}_2'}. \tag{3.51}$$

Moreover, as detailed in Appendix C.2, using these results we can show that

$$\overline{\nabla\times\left(\rho_1'\partial_t\boldsymbol{u}_2' + \rho_2'\partial_t\boldsymbol{u}_1'\right)} = \boldsymbol{0}. \tag{3.52}$$

3.8. *Steady streaming at $O(\epsilon^2)$ (part 2)*

Now that the forcing terms involving the $O(\epsilon^2)$ acoustic fields have been computed, the streaming flow can be evaluated. The equation for the stream function reduces to

$$\frac{1}{Re}\nabla^4\overline{\psi}_2 = \underbrace{\overline{u_1'\partial_x\Omega_2'}}_{B} - \underbrace{\overline{\delta\, v_{3/2}'\partial_t\mathbb{F}_{3/2}'}}_{F}, \tag{3.53}$$

with the baroclinic and external forcing terms respectively defined as

$$B \equiv \overline{u_1'\partial_x\Omega_2'} = -\frac{\mathbb{A}^2\Gamma}{4\delta\gamma^2}\sin(2x), \qquad F \equiv -\overline{\delta v_{3/2}'\partial_t\mathbb{F}_{3/2}'} = -\delta\left(y - \frac{1}{2}\right)\left|\mathbb{F}_{3/2}\right|^2\sin(2x). \tag{3.54}$$

This equation is supplemented with the following no-penetration and slip velocity conditions:

$$\partial_x\overline{\psi}_2(x, y=0) = \partial_x\overline{\psi}_2(x, y=1) = 0, \qquad \partial_y\overline{\psi}_2(x, y=0) = \partial_y\overline{\psi}_2(x, y=1) = \delta\overline{u}_{slip}, \tag{3.55}$$

with $\overline{u}_{slip}$ reported in (3.41). An explicit solution for $\overline{\psi}_2$ can be computed; a representative velocity field is shown in figure 2(*a*) for a specific set of dimensionless parameters.

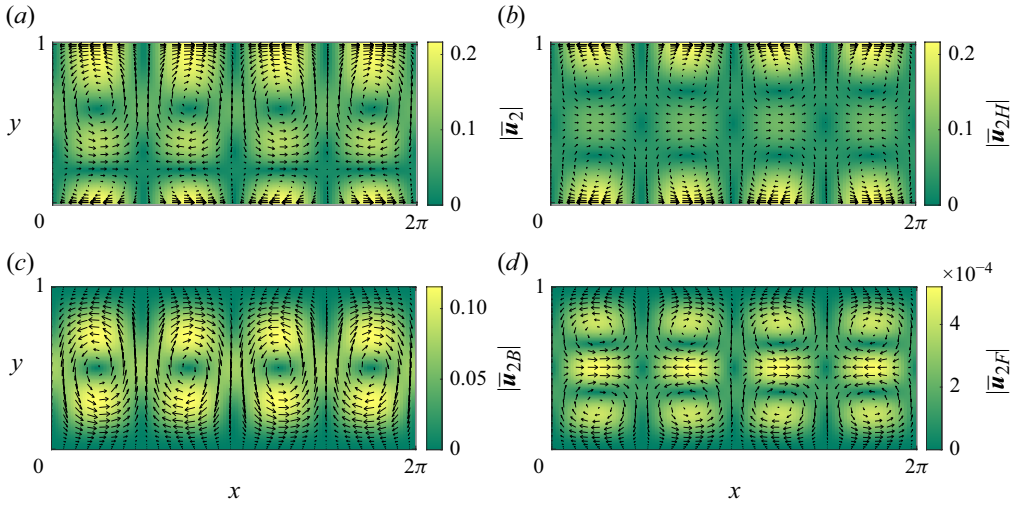

Figure 2. Visualisation of the strength and orientation of the streaming velocity field in the channel interior. (*a*) The total velocity field $\overline{\boldsymbol{u}}_2$, (*b*) the homogeneous Rayleigh streaming component $\overline{\boldsymbol{u}}_{2H}$, (*c*) the baroclinic contribution $\overline{\boldsymbol{u}}_{2B}$ and (*d*) the inhomogeneous component $\overline{\boldsymbol{u}}_{2F}$ resulting from the specified external body force. Components $\overline{\boldsymbol{u}}_{2H}$ and $\overline{\boldsymbol{u}}_{2F}$ have stacked multicellular structure while a single pair of cells that spans the channel interior is manifest in $\overline{\boldsymbol{u}}_{2B}$. The components $\overline{\boldsymbol{u}}_{2H}$, $\overline{\boldsymbol{u}}_{2F}$ and $\overline{\boldsymbol{u}}_{2B}$ possess wall-normal symmetry about the mid-plane, which is not reflected in the total velocity field $\overline{\boldsymbol{u}}_2$. The parameters correspond to $A = 1$, $Re = 500$, $Pr = 0.71$, $\delta = 1$, $\gamma = 1.4$ and $\Gamma = \Gamma_c = 0.278$ (Γ_c is defined in § 4.2).

To gain physical insight into the various contributions generating this streaming flow, it is instructive to split the stream function into three components:

$$\overline{\psi}_2 = \overline{\psi}_{2H} + \overline{\psi}_{2B} + \overline{\psi}_{2F}, \tag{3.56}$$

where these functions (explicitly reported in Appendix D) have the following properties.

(i) Component $\overline{\psi}_{2H}$ is the solution of the homogeneous partial differential equation $\boldsymbol{\nabla}^4\overline{\psi}_{2H} = 0$ with the full boundary conditions (3.55). This component corresponds to the extension to $O(1)$ aspect ratio of the solution obtained by Rayleigh for fluids of uniform (mean) temperature. As shown in figure 2(*b*), the velocity field consists of stacked counter-rotating cells and is symmetric with respect to $y = 1/2$. This contribution is independent of the imposed temperature difference Γ.

(ii) Component $\overline{\psi}_{2B}$ is the solution of the inhomogeneous partial differential equation $\boldsymbol{\nabla}^4\overline{\psi}_{2B} = Re\,\mathrm{B}$, with no-penetration and no-slip boundary conditions ($\partial_x\overline{\psi}_{2B}(x,\, y = 0) = \partial_x\overline{\psi}_{2B}(x,\, y = 1) = \partial_y\overline{\psi}_{2B}(x,\, y = 0) = \partial_y\overline{\psi}_{2B}(x,\, y = 1) = 0$). It is the only component $\overline{\psi}_{2B}$ that involves the temperature difference Γ and therefore describes the baroclinic component of the streaming flow. This component consists of a cellular flow that spans the entire height of the channel; see figure 2(*c*).

(iii) Component $\overline{\psi}_{2F}$ is the solution of the inhomogeneous partial differential equation $\boldsymbol{\nabla}^4\overline{\psi}_{2F} = Re\,\mathrm{F}$, subject to no-penetration and no-slip boundary conditions. This component of the flow depends on the details of the wave forcing mechanism, and would differ if the acoustic wave were generated by an oscillating wall rather than by an external body force. (A periodic motion of a solid boundary also generates streaming (Lighthill 1978).) However, this contribution is found to be negligible for the set of dimensionless parameters considered here, as for instance evident in figure 2(*d*).

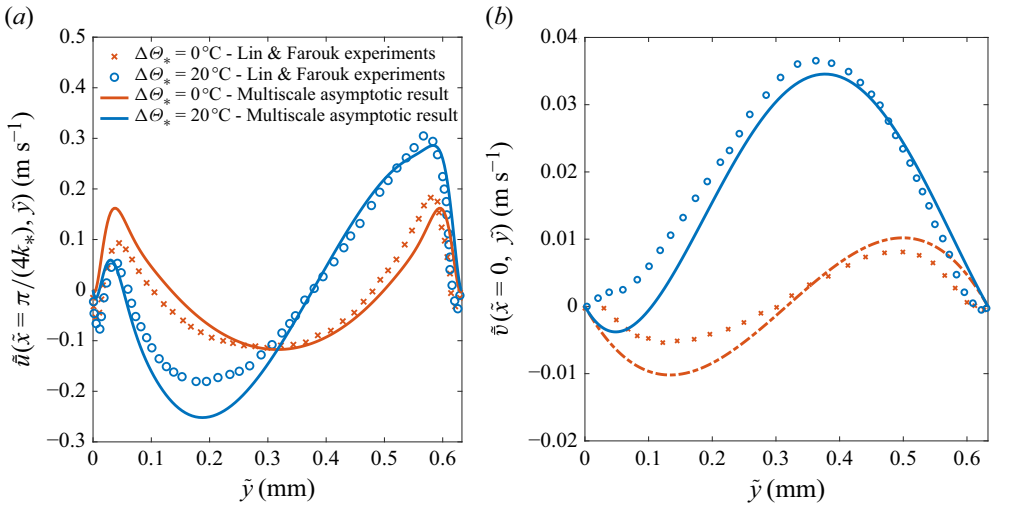

Figure 3. Comparison of the present analytical solution with the (*a*) x and (*b*) y components of the streaming velocity field (at $\tilde{x} = \pi/(4k_*)$ and $\tilde{x} = 0$ respectively) from the DNS performed by Lin & Farouk (2008) (their cases 1A and 1B). The full composite solution representing the dynamics in the BLs as well as the interior is shown by the solid curves. The parameters correspond to $A = 6.37$, $Re = 631$, $Pe = 448$, $\delta = 0.2252$, $\gamma = 5/3$, $\epsilon = 10^{-2}$ and $\Gamma = \{0, 6.67\}$. For these parameters, the critical temperature difference $\Gamma_c = 4.45$, i.e. $\Delta\Theta_{*_c} \approx 13.4\,°C$ (Γ_c is defined in § 4.2).

4. Validation, results and discussion

4.1. *Comparison with previous studies*

The streaming flow derived in § 3.8 is now compared with other theoretical and numerical solutions reported in the literature. In the absence of an external temperature difference and thermal diffusion, the solution converges to that derived by Rayleigh in the limit of narrow channels. Specifically, as discussed in § 3.6, the slip velocity in the absence of thermal diffusion reads $\overline{u}_{slip_*} = -[3U_0^2/(8a_*)]\sin(2k_*\tilde{x})$. Since, in the limit $\delta \to 0$, $\overline{\psi}_{2H} \to -\delta\,\overline{u}_{slip}\,y\,(2y^2 - 3y + 1)$, the corresponding leading-order dimensional streaming velocity becomes

$$\tilde{\overline{u}}_H \sim \frac{3U_0^2}{16a_*}\sin(2k_*\tilde{x})\left[1 - 3\left(\frac{(H_*/2) - \tilde{y}}{(H_*/2)}\right)^2\right], \tag{4.1}$$

$$\tilde{\overline{v}}_H \sim \frac{3U_0^2}{16a_*}2k_*\cos(2k_*\tilde{x})\left[\frac{H_*}{2} - \tilde{y} - \frac{(H_*/2 - \tilde{y})^3}{(H_*/2)^2}\right], \tag{4.2}$$

which are the same as (93)–(94) in Rayleigh (1884) (except for the signs since Rayleigh considered an acoustic velocity field $\propto \cos(k_*\tilde{x})$ whereas it is here $\propto \sin(k_*\tilde{x})$).

When a finite temperature difference is imposed ($\Gamma \neq 0$), the solution derived in the current work can be compared with DNS of the compressible Navier–Stokes equations performed by Lin & Farouk (2008); see figure 3. To account for the finite width of the oscillatory BLs of the DNS, a composite analytical solution (Van Dyke 1969) is obtained by adding the streaming velocity profile in the BLs (§ 3.6) with that in the interior (§ 3.8). Reasonable agreement is observed, some discrepancy being expected since the DNS employs a different forcing mechanism (an oscillating wall) and incorporates variations of viscosity and thermal conductivity with temperature. In this regime, a qualitative

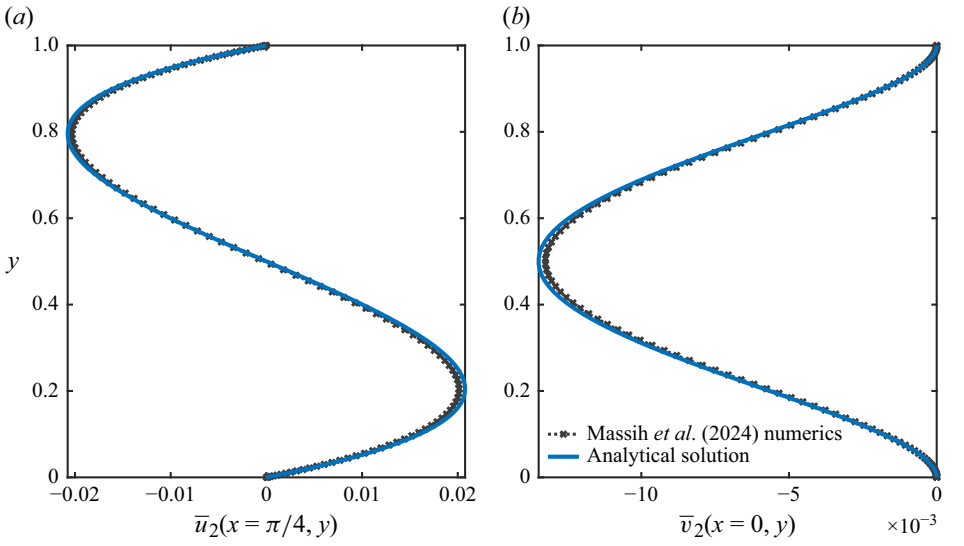

Figure 4. Comparison of the present analytical solution with the (*a*) x and (*b*) y components of the streaming velocity field (at $x=\pi/4$ and $x=0$ respectively) obtained using the two-way coupled numerical algorithm of Massih *et al.* (2024) that assumes $\hat{\Gamma}=O(1)$ (instead of $\hat{\Gamma}=O(\epsilon)$ for the present analysis). The parameters correspond to $A=0.01$, $Re=2500$, $Pe=1775$, $\delta=1$, $\gamma=1.4$, $\epsilon=3\times10^{-4}$ and $\hat{\Gamma}=\epsilon\Gamma=0.03\gg\epsilon\Gamma_c$ (Γ_c, defined in § 4.2, is 0.056 for this set of parameters).

comparison also is subsequently made with the experimental observations of Nabavi *et al.* (2008).

For even larger imposed temperature differences $\hat{\Gamma}=\Delta\Theta_*/T_*$, we compare the solution derived in this work assuming $\hat{\Gamma}=\epsilon\Gamma$, with $\Gamma=O(1)$, with the numerical results obtained by Massih *et al.* (2024) in the asymptotic limit $\hat{\Gamma}=O(1)$. For this comparison, we consider a finite temperature difference of $\hat{\Gamma}=0.03$, treated as $O(1)$ in the numerical algorithm of Massih *et al.* (2024) and as $\Gamma=0.03/\epsilon$ in the current framework, all the other dimensionless parameters being identical ($A=0.01$, $Re=2500$, $Pe=1775$, $\delta=1$ and $\gamma=1.4$). The small parameter ϵ is arbitrarily set to 3×10^{-4}. The wall-normal profiles of the x and y streaming velocity components in the interior of the domain are shown in figure 4. The new asymptotic model captures the numerical results, with the accuracy improving in the limit $\epsilon\to0$, as expected. In this strongly stratified limit, the streaming velocity field is largely dominated by the baroclinic component $\overline{\boldsymbol{u}}_{2B}$, with the other components being orders of magnitude smaller for the chosen parameter values.

4.2. *Critical non-dimensional temperature difference Γ_c*

Figure 5 shows the interior streamlines of the streaming flow, with the magnitude of the streaming velocity $|\overline{\boldsymbol{u}}_2|$ shown in colour, for domains of aspect ratio $\delta=1$ and $\delta=10$. The analytical solution captures the evolution of the structure and intensity of the streaming flow as the temperature difference increases. A parametric threshold can be defined to quantify the transition from the stacked multicellular Rayleigh streaming to the unicellular baroclinic acoustic streaming, i.e. from $\overline{\boldsymbol{u}}_{2H}=\boldsymbol{\nabla}\times(\overline{\psi}_{2H}\boldsymbol{e}_z)$ to $\overline{\boldsymbol{u}}_{2B}=\boldsymbol{\nabla}\times(\overline{\psi}_{2B}\boldsymbol{e}_z)$. To that end, we define a kinetic energy parameter for each component of the streaming flow:

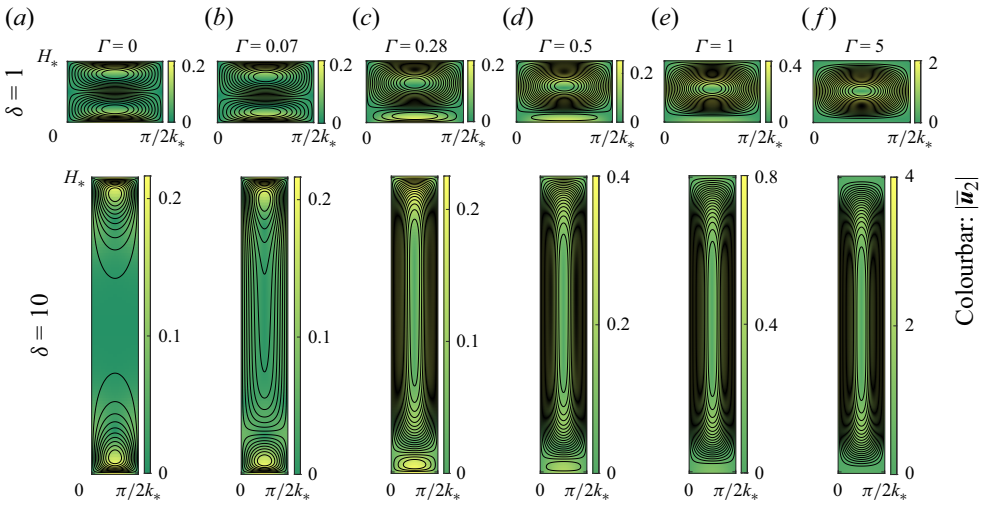

Figure 5. Streaming flow for $A = 1$, $Re = 500$, $Pr = 0.71$, $\gamma = 1.4$, $\delta = \{1, 10\}$ and (*a*) $\Gamma = 0$, (*b*) $\Gamma = 0.07$, (*c*) $\Gamma = 0.28$, (*d*) $\Gamma = 0.5$, (*e*) $\Gamma = 1$ and (*f*) $\Gamma = 5$. The streaming velocity increases with the imposed temperature difference, while the cells closer to the hot boundary expand vertically and those closer to the cold wall shrink. For this set of parameters, $\Gamma_c(\delta = 1) = 0.28$ and $\Gamma_c(\delta = 10) = 0.07$. The ($x$) width of the domain plotted corresponds to one half of an acoustic wave wavelength.

$$K_H \equiv \frac{1}{\pi}\int_0^{2\pi}\int_0^1 |\overline{\boldsymbol{u}}_{2H}|^2 \,\mathrm{d}x\,\mathrm{d}y = \frac{1}{\pi}\int_0^{2\pi}\int_0^1 \left|\boldsymbol{\nabla}\overline{\psi}_{2H}\right|^2 \mathrm{d}x\mathrm{d}y, \tag{4.3}$$

$$K_B \equiv \frac{1}{\pi}\int_0^{2\pi}\int_0^1 |\overline{\boldsymbol{u}}_{2B}|^2 \,\mathrm{d}x\,\mathrm{d}y = \frac{1}{\pi}\int_0^{2\pi}\int_0^1 \left|\boldsymbol{\nabla}\overline{\psi}_{2B}\right|^2 \mathrm{d}x\mathrm{d}y, \tag{4.4}$$

$$K_F \equiv \frac{1}{\pi}\int_0^{2\pi}\int_0^1 |\overline{\boldsymbol{u}}_{2F}|^2 \,\mathrm{d}x\,\mathrm{d}y = \frac{1}{\pi}\int_0^{2\pi}\int_0^1 \left|\boldsymbol{\nabla}\overline{\psi}_{2F}\right|^2 \mathrm{d}x\mathrm{d}y. \tag{4.5}$$

The analytical expressions for these coefficients are reported in Appendix E. Note that $|\overline{\boldsymbol{u}}_2|^2 \neq |\overline{\boldsymbol{u}}_{2H}|^2 + |\overline{\boldsymbol{u}}_{2B}|^2 + |\overline{\boldsymbol{u}}_{2F}|^2$. Since only K_B depends on Γ, a critical temperature difference Γ_c can be defined such that

$$K_H\,(\delta,\, Re,\, Pr,\, \gamma,\, A) = K_B\,(\Gamma = \Gamma_c,\, \delta,\, Re,\, Pr,\, \gamma,\, A)\,. \tag{4.6}$$

For the set of parameters reported in figure 5, $\Gamma_c = 0.28$ for $\delta = 1$ and $\Gamma_c = 0.07$ for $\delta = 10$, which qualitatively corresponds to a hot cell that spans around 80 % of the height of the channel. The dependence of Γ_c on other independent parameters can also be investigated. Using the expressions reported in Appendix E,

$$\begin{aligned} K_H &= \mathbb{A}^4\gamma^{-4}\left[1 + Pr + 2(\gamma-1)\sqrt{Pr}/3\right]^2 (1+Pr)^{-2} F_H(\delta), \\ K_B &= \mathbb{A}^4\Gamma^2 Re^2\gamma^{-4} F_B(\delta), \end{aligned} \tag{4.7}$$

and therefore

$$\hat{\Gamma}_c = \epsilon\,\Gamma_c = \frac{1}{Re_w}\left(1 + \frac{2(\gamma-1)\sqrt{Pr}}{3(1+Pr)}\right) F_c(\delta) \tag{4.8}$$

is notably independent of the wave amplitude $\mathbb{A}$ and inversely proportional to $Re_w = \rho_*\, a_*/(k_*\,\mu_*)$. The terms grouped in parentheses represent the dependence of Γ_c on the

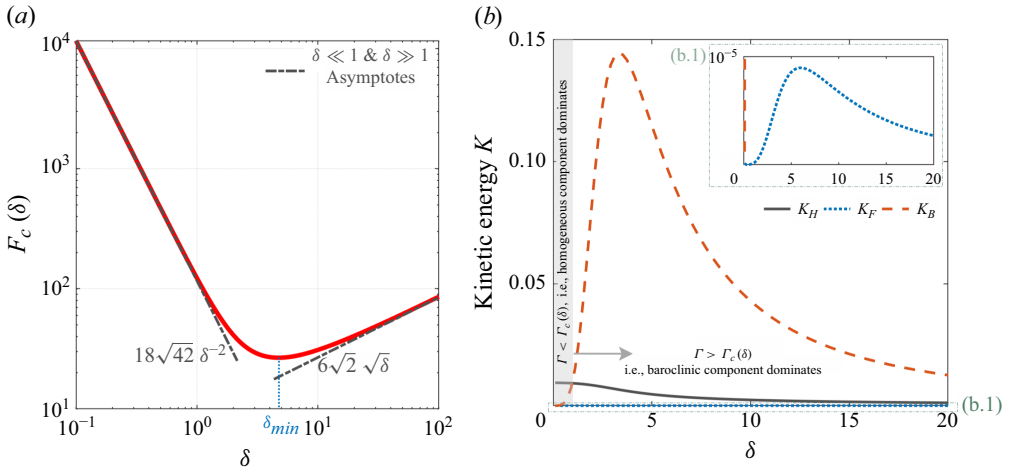

Figure 6. (*a*) Aspect-ratio dependence of the function F_c to which the critical temperature difference Γ_c is proportional (see (4.8)). As the imposed temperature difference increases, the transition from Rayleigh to baroclinic streaming first occurs at $\delta = \delta_{min} = 4.74$. In the narrow channel limit the critical temperature difference $\Gamma_c = O(\delta^{-2})$, while in the tall channel limit the critical temperature difference $\Gamma_c = O(\sqrt{\delta})$ (see (4.9)). (*b*) Kinetic energy parameters K_H, K_F and K_B as functions of the aspect ratio δ ($A = 1$, $\Gamma = 0.5$, $Re = 300$, $Pr = 0.71$ and $\gamma = 1.4$).

fluid properties. The dependence of Γ_c on the channel geometry (δ) is non-monotonic: F_c has a minimum for $\delta = \delta_{min} = 4.74$ and satisfies

$$F_c(\delta_{min}) = 26.68, \qquad F_c(\delta) \underset{\delta \ll 1}{\simeq} 18\sqrt{42}\,\delta^{-2}, \qquad F_c(\delta) \underset{\delta \gg 1}{\simeq} 6\sqrt{2}\,\sqrt{\delta}. \tag{4.9}$$

The dependence of F_c and each of the kinetic energy parameters on the aspect ratio δ is shown in figure 6. In particular, the kinetic energy parameter corresponding to the specific acoustic wave forcing mechanism, K_F, is found to be several orders of magnitude smaller than the others. The most consequential result is that Γ_c is minimum for $\delta_{min} = 4.74$ independently of all the other dimensionless parameters and significantly increases as δ departs from this value. This knowledge should prove valuable for the design of an experimental set-up aiming to show this transition near δ_{min}. In cases where streaming flows are undesirable, our result highlights the extreme sensitivity of channels of aspect ratios near this value to external temperature differences.

To further emphasise the role of Γ_c in dictating the flow morphology, we qualitatively analyse the observations of Nabavi *et al.* (2008), who report experimental measurements of the streaming flow in an acoustic resonator subject to external temperature differences. For the set of dimensionless parameters considered by those authors ($A = 7$, $Re = 1236.5$, $Pe = 953$, $\delta = 0.7$, $\gamma = 1.4$ and $\epsilon = 10^{-3}$), we compute $\Gamma_c = 0.214$, corresponding to a dimensional critical temperature difference $\Delta\Theta_{c_*} = 0.06\ ^\circ\mathrm{C}$ across the channel. Although the experimental regime (particularly $Re = 1236.5 \approx 1/\epsilon$ and $Pe = 953 \approx 1/\epsilon$) seemingly falls outside the range of asymptotic validity of the current analysis, the analytical results presented here nevertheless capture the transition that was found to occur between $\Delta\Theta_* = 0\ ^\circ\mathrm{C}$ and $\Delta\Theta_* = 0.3\ ^\circ\mathrm{C}$. In fact, knowledge of the critical temperature difference Γ_c could be used to inform future experiments aiming to precisely track the transition in flow morphology. Figure 7(*a*) compares the wall-normal structure of the interior horizontal streaming velocity $\overline{u}_2$ for different temperature differences $\Delta\Theta_* = \{0, 0.06, 0.3\}\ ^\circ\mathrm{C}$. The corresponding normalised velocity fields are also shown in figure 7(*b*). The fields obtained

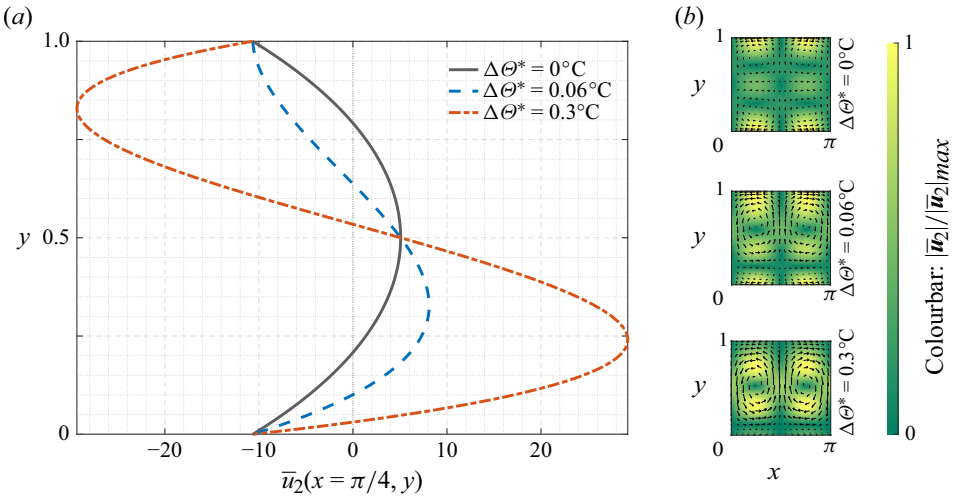

Figure 7. Streaming flow predicted for the dimensionless parameters reported in Nabavi *et al.* (2008): $A = 7$, $Re = 1236.5$, $Pe = 953$, $\delta = 0.7$, $\gamma = 1.4$ and $\epsilon = 10^{-3}$. (*a*) Vertical profile of the interior horizontal streaming velocity $\overline{u}_2(x = \pi/4,\ y)$ and (*b*) normalised streaming velocity field $|\overline{\boldsymbol{u}}_2|/|\overline{\boldsymbol{u}}_2|_{max}$ and velocity vectors for $\Gamma = 0$ ($\Delta\Theta_* = 0$ °C), $\Gamma = \Gamma_c = 0.214$ ($\Delta\Theta_{c_*} = 0.06$ °C) and $\Gamma = 1$ ($\Delta\Theta_* = 0.3$ °C). For this set of parameters, $\Gamma_c = 0.214$ ($\Delta\Theta_{c_*} = 0.06$ °C) lies in the transition range evident in figure 4 of Nabavi *et al.* (2008).

for $\Delta\Theta_* = 0$ °C and $\Delta\Theta_* = 0.3$ °C compare well with the experimental results reported in Nabavi *et al.* (2008).

5. Conclusion

In this investigation we analyse the streaming flows generated by a standing acoustic wave in a channel with hot and cold walls held at fixed but differing temperatures (respectively $T_* + \Delta\Theta_*$ and T_*). Using asymptotic approximations, an analytical solution is derived that characterises the smooth transition from Rayleigh streaming to baroclinic acoustic streaming. This solution accounts for prior experimental and numerical observations: as the temperature difference increases, the stacked cellular structure characteristic of Rayleigh streaming transforms to a unicellular structure, in which the cells span the height of the channel and streaming velocities are enhanced significantly. The present study enables the extensive exploration of this transition by providing an analytical expression for the associated acoustic wave and streaming fields.

In this intermediate regime, the streaming flow $\overline{\boldsymbol{u}}_2$ is expressed as the sum of three contributions. The first, $\overline{\boldsymbol{u}}_{2H}$, is driven by viscous torques in the oscillatory BLs and extends the solution derived by Rayleigh to $O(1)$ aspect ratios. The second, $\overline{\boldsymbol{u}}_{2B}$, is directly proportional to the imposed temperature difference and, in particular, is directly related to the acoustic wave vorticity generated baroclinically in the interior of the channel. The third contribution, $\overline{\boldsymbol{u}}_{2F}$, depends on the details of the wave forcing mechanism and in practice is found to be negligible. A critical temperature difference $\Delta\Theta_{c_*}$ can be defined based on equating the kinetic energies of the viscous and baroclinically driven streaming flows to quantify the transition from $\overline{\boldsymbol{u}}_{2H}$ to $\overline{\boldsymbol{u}}_{2B}$ as $\Delta\Theta_*$ is increased. We show that

$$\Delta\Theta_{c_*} = \epsilon\ \Gamma_c\ T_* = \frac{k_*\mu_*}{\rho_* a_*}\frac{\left[1 + \dfrac{\mu_* c_{p*}}{\kappa_*} + \dfrac{2}{3}\left(\dfrac{c_{p*}}{c_{v*}} - 1\right)\sqrt{\dfrac{\mu_* c_{p*}}{\kappa_*}}\right]}{1 + \dfrac{\mu_* c_{p*}}{\kappa_*}} F_c(k_* H_*)\ T_*, \qquad (5.1)$$

Attribute	Rayleigh streaming (RS)	Transition from RS to BAS	Baroclinic acoustic streaming (BAS)
Schematic	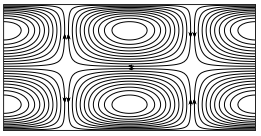	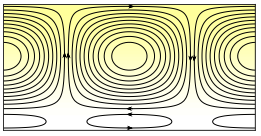	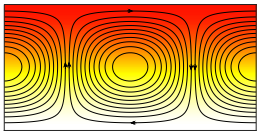
Temperature difference	$\Delta\Theta_* \ll \Delta\Theta_{c_*}$	$\Delta\Theta_* = O(\Delta\Theta_{c_*})$	$\Delta\Theta_* \gg \Delta\Theta_{c_*}$
Streaming velocity scale	$U_{s_*} = U_*^2/a_*$	$U_{s_*} = U_*^2/a_*$	$U_{s_*} = U_*$
Driving mechanism	Attenuation (BLs) and wave forcing mechanism	Baroclinicity (interior), attenuation (BLs) and wave forcing mechanism	Baroclinicity (interior)
Features	Stacked cells and symmetry about $\tilde{y} = H_*/2$	Stacked cells and no symmetry about $\tilde{y} = H_*/2$	Single cell and no symmetry about $\tilde{y} = H_*/2$ (see Massih *et al.* 2024)
Solution	Asymptotic analytical approximations exist	Asymptotic analytical approximations exist	Numerical solution only
Dynamics	The waves drive a mean flow. No feedback from the mean flow	The waves drive a mean flow. No feedback from the mean flow	The waves drive a mean flow. The mean flow affects the waves

Table 3. Summary of acoustic streaming regimes in a differentially heated channel. Recall that U_* is the typical acoustic wave velocity, a_* the speed of sound, $\Delta\Theta_*$ the temperature difference across the channel of height H_* and $\Delta\Theta_{c_*}$ the critical temperature difference given in (5.1).

where F_c is an explicit function that has a minimum value of 27 for $k_*H_* = 4.74$. For air at standard temperature and pressure as a working fluid ($T_* = 273$ K, $\mu_* = 1.7 \times 10^{-5}$ kg (m s)$^{-1}$, $\rho_* = 1.3$ kg m^{-3}, $c_{p*} = 1.0 \times 10^3$ J (kg K)$^{-1}$, $c_{v*} = c_{p*}/1.4$, $\kappa_* = 0.024$ W (m K)$^{-1}$, $a_* = 331$ m s^{-1}), a channel of height $H_* = 1$ cm and an acoustic wave of wavenumber $k_* = 4.74/H_* = 474$ m^{-1} (and, thus, $f_* = k_*a_*/(2\pi) = 25$ kHz), we find $\Delta\Theta_{c_*} = 0.15$ K. Larger channel heights with the same aspect ratio would further reduce this critical temperature difference (for $H_* = 10$ cm and $k_* = 4.74/H_*$, $\Delta\Theta_{c_*} = 15$ mK). This estimate demonstrates the extreme sensitivity of streaming flows in a gas to temperature inhomogeneities.

The estimation of this transitional temperature gradient also aids in the design of experiments. First, $\Delta\Theta_{c_*}$ should be computed and compared with the actual temperature difference $\Delta\Theta_*$. If $\Delta\Theta_* \ll \Delta\Theta_{c_*}$, baroclinicity can be neglected and Rayleigh's approach for homogeneous fluids used. For $\Delta\Theta_* = O(\Delta\Theta_{c_*})$, the present analytical solution should be employed, whereas a larger temperature difference $\Delta\Theta_* \gg \Delta\Theta_{c*}$ generates two-way coupling between the waves and the streaming flows that is captured in the framework developed in Chini *et al.* (2014), Michel & Chini (2019) and Massih *et al.* (2024). Table 3 compares these various regimes of acoustic streaming in a gas and highlights the transition from Rayleigh streaming to baroclinic acoustic streaming.

Declaration of interests. The authors report no conflict of interest.

Appendix A. Analytical solutions for the acoustic waves at $O(\epsilon^{3/2})$

The $O(\epsilon^{3/2})$ acoustic fields in the interior are

$$\pi'_{3/2} = [(\delta^2\gamma\mathbb{F}_{3/2}/2)y^2 + C_1 y + C_2]\cos(x)\,\mathrm{e}^{\mathrm{i}t} + \text{c.c.} \quad \text{(interior)}, \tag{A1}$$

$$u'_{3/2} = \mathrm{i}\gamma^{-1}[(\delta^2\gamma\mathbb{F}_{3/2}/2)y^2 + C_1 y + C_2 + \mathbb{F}_{3/2}\gamma]\sin(x)\,\mathrm{e}^{\mathrm{i}t} + \text{c.c.} \quad \text{(interior)}, \tag{A2}$$

$$v'_{3/2} = \mathrm{i}(\gamma\delta^2)^{-1}[(\delta^2\gamma\mathbb{F}_{3/2})y + C_1]\cos(x)\,\mathrm{e}^{\mathrm{i}t} + \text{c.c.} \quad \text{(interior)}, \tag{A3}$$

$$\Theta'_{3/2} = (1-\gamma^{-1})\pi'_{3/2} \quad \text{(interior)}, \tag{A4}$$

$$\rho'_{3/2} = \gamma^{-1}\pi'_{3/2} \quad \text{(interior)}. \tag{A5}$$

The vertical velocity field $v'_{3/2}$ evaluated at $y=0$ in the interior (A3) must match the value obtained in the cold-wall BL as $\eta\to\infty$ (3.21) and analogously at $y=1$. This matching is achieved by setting

$$C_1 = -\frac{\delta^2\gamma}{2}\mathbb{F}_{3/2}, \qquad \mathbb{F}_{3/2} = (1-i)\,\frac{\mathbb{A}}{2\,\gamma}\left(\frac{(\gamma-1)}{\sqrt{\mathbb{P}}} + \frac{1}{\sqrt{\mathbb{R}}}\right). \tag{A6}$$

The constant C_2 seemingly remains undetermined at this stage. We determine C_2 by noting that the corresponding acoustic field has exactly the same form as that obtained at $O(\epsilon)$, consisting of a plane horizontal wave with BLs to satisfy the no-slip and isothermal boundary conditions. Thus, the wave solution associated with the constant C_2 merely corresponds to an $O(\epsilon)$ modification of the leading-order acoustic wave amplitude $\mathbb{A}$ and does not encapsulate any new physical phenomena. Accordingly, we choose to set $C_2 = -\gamma\mathbb{F}_{3/2}$ to ensure a zero oscillatory horizontal velocity in the interior close to each boundary and thereby obviate the need for mechanical BLs at this order. The thermal boundary layer, however, remains and the following expression for the fields close to the walls is obtained:

$$\pi'_{3/2} = -\gamma\mathbb{F}_{3/2}\cos(x)\mathrm{e}^{\mathrm{i}t} + \text{c.c.} \quad \text{(BLs)}, \tag{A7}$$

$$u'_{3/2} = 0 \quad \text{(BLs)}, \tag{A8}$$

$$v'_2 = \begin{cases} \mathbb{F}_{3/2}\left[\mathrm{i}\eta + \dfrac{(1+\mathrm{i})}{2\sqrt{\mathbb{P}}}(\gamma-1)(1-\mathrm{e}^{-(1+\mathrm{i})\sqrt{\mathbb{P}}\eta})\right]\cos(x)\mathrm{e}^{\mathrm{i}t} + \text{c.c.} \quad \text{(C-BL)} \\ -\mathbb{F}_{3/2}\left[\mathrm{i}\eta + \dfrac{(1+\mathrm{i})}{2\sqrt{\mathbb{P}}}(\gamma-1)(1-\mathrm{e}^{-(1+\mathrm{i})\sqrt{\mathbb{P}}\eta})\right]\cos(x)\,\mathrm{e}^{\mathrm{i}t} + \text{c.c.} \quad \text{(H-BL)}, \end{cases} \tag{A9}$$

$$\Theta'_{3/2} = -\mathbb{F}_{3/2}(\gamma-1)\left[1-\mathrm{e}^{-(1+\mathrm{i})\sqrt{\mathbb{P}}\eta}\right]\cos(x)\,\mathrm{e}^{\mathrm{i}t} + \text{c.c.} \quad \text{(BLs)}, \tag{A10}$$

$$\rho'_{3/2} = -\mathbb{F}_{3/2}\left[1+(\gamma-1)\mathrm{e}^{-(1+\mathrm{i})\sqrt{\mathbb{P}}\eta}\right]\cos(x)\,\mathrm{e}^{\mathrm{i}t} + \text{c.c.} \quad \text{(BLs)}. \tag{A11}$$

Appendix B. Leading-order streaming flow in the BLs

The leading-order streaming flow in the BLs is explicitly given by

$$\begin{aligned}\overline{u}_2 = \frac{\mathbb{A}^2\sin(2x)\mathrm{e}^{-[(1+\mathrm{i})(\sqrt{\mathbb{P}}+\sqrt{\mathbb{R}})+\sqrt{\mathbb{R}}]\eta}}{8\gamma^2\mathbb{P}(\mathbb{P}+\mathbb{R})}\Big\{ &-\mathrm{i}(\gamma-1)\mathbb{R}(\mathbb{P}+\mathbb{R})\mathrm{e}^{(2+\mathrm{i})\sqrt{\mathbb{R}}\eta} \\ &+\mathbb{P}(\mathbb{P}+\mathbb{R})\mathrm{e}^{[(1+\mathrm{i})\sqrt{\mathbb{P}}+\mathrm{i}\sqrt{\mathbb{R}}]\eta} + \mathrm{i}(\gamma-1)\mathbb{R}(\mathbb{P}+\mathbb{R})\mathrm{e}^{[2\mathrm{i}\sqrt{\mathbb{P}}+(2+\mathrm{i})\sqrt{\mathbb{R}}]\eta} \\ &-(\gamma-1)\mathbb{R}[(\sqrt{\mathbb{P}\mathbb{R}}+\mathrm{i}\mathbb{P})\mathrm{e}^{(\sqrt{\mathbb{R}}+2\mathrm{i}\sqrt{\mathbb{P}})\eta} + (\sqrt{\mathbb{P}\mathbb{R}}-\mathrm{i}\mathbb{P})\mathrm{e}^{(1+2\mathrm{i})\sqrt{\mathbb{R}}\eta}] \\ &+\sqrt{\mathbb{P}}(\mathbb{P}+\mathbb{R})[(\gamma-1)\sqrt{\mathbb{R}}+(1+3\mathrm{i})\sqrt{\mathbb{P}}]\mathrm{e}^{[\sqrt{\mathbb{R}}+(1+\mathrm{i})\sqrt{\mathbb{P}}]\eta}\end{aligned}$$

$$-\mathbb{P}[2(\gamma-1)\sqrt{\mathbb{PR}}+3(\mathbb{P}+\mathbb{R})]\mathrm{e}^{[(1+\mathrm{i})(\sqrt{\mathbb{P}}+\sqrt{\mathbb{R}})+\sqrt{\mathbb{R}}]\eta}$$
$$+\sqrt{\mathbb{P}}(\mathbb{P}+\mathbb{R})[(\gamma-1)\sqrt{\mathbb{R}}+(1-3\mathrm{i})\sqrt{\mathbb{P}}]\mathrm{e}^{[(1+\mathrm{i})\sqrt{\mathbb{P}}+(1+2\mathrm{i})\sqrt{\mathbb{R}}]\eta}\Big\}. \tag{B1}$$

Appendix C. Simplification of the torques driving the streaming flow

C.1. *Using vector identities and equations at lower order*

Various nonlinear terms in the expression for the stream function (obtained by taking the curl of (3.42)) can be simplified. In particular, since the acoustic vorticity in the interior vanishes at $O(\epsilon^{3/2})$,

$$\boldsymbol{\nabla}\times\left[(\boldsymbol{u}'_{3/2}\cdot\boldsymbol{\nabla})\boldsymbol{u}'_{3/2}\right]=\boldsymbol{\nabla}\times\left[\frac{1}{2}\,\boldsymbol{\nabla}(\boldsymbol{u}'_{3/2}\cdot\boldsymbol{u}'_{3/2})+(\boldsymbol{\nabla}\times\boldsymbol{u}'_{3/2})\times\boldsymbol{u}'_{3/2}\right]=\boldsymbol{0}. \tag{C1}$$

Similarly, exploiting vector identities and that $\boldsymbol{\Omega}'_{\boldsymbol{1}}=\boldsymbol{0}$ in the interior yields both

$$\begin{aligned}\boldsymbol{\nabla}\times\left[(\boldsymbol{u}'_1\cdot\boldsymbol{\nabla})\boldsymbol{u}'_2+(\boldsymbol{u}'_2\cdot\boldsymbol{\nabla})\boldsymbol{u}'_1\right]&=\boldsymbol{\nabla}\times\left[\boldsymbol{\nabla}(\boldsymbol{u}'_2\cdot\boldsymbol{u}'_1)+(\boldsymbol{\nabla}\times\boldsymbol{u}'_2)\times\boldsymbol{u}'_1+(\boldsymbol{\nabla}\times\boldsymbol{u}'_1)\times\boldsymbol{u}'_2\right]\\&=\boldsymbol{\nabla}\times(\boldsymbol{\Omega}'_2\times\boldsymbol{u}'_1)\end{aligned} \tag{C2}$$

and

$$\begin{aligned}2\boldsymbol{\nabla}\times\left[\overline{\rho}_1(\boldsymbol{u}'_1\cdot\boldsymbol{\nabla})\boldsymbol{u}'_1\right]&=\boldsymbol{\nabla}\times\left[\overline{\rho}_1\boldsymbol{\nabla}(\boldsymbol{u}'_1\cdot\boldsymbol{u}'_1)+2\,\overline{\rho}_1(\boldsymbol{\nabla}\times\boldsymbol{u}'_1)\times\boldsymbol{u}'_1\right]\\&=\boldsymbol{\nabla}\times\left[\overline{\rho}_1\boldsymbol{\nabla}(\boldsymbol{u}'_1\cdot\boldsymbol{u}'_1)\right]=(\boldsymbol{\nabla}\overline{\rho}_1)\times\left[\boldsymbol{\nabla}(\boldsymbol{u}'_1\cdot\boldsymbol{u}'_1)\right].\end{aligned} \tag{C3}$$

The nonlinear term involving the $O(\epsilon^{3/2})$ acoustic fields does not vanish and can be related to the external force density $\mathbb{F}'_{3/2}$ with the use of (3.24) and (A5):

$$\begin{aligned}\boldsymbol{\nabla}\times(\rho'_{3/2}\partial_t\boldsymbol{u}'_{3/2})&=\boldsymbol{\nabla}\times\left(\gamma^{-1}\pi'_{3/2}\left[-\gamma^{-1}\boldsymbol{\nabla}\pi'_{3/2}+\mathbb{F}'_{3/2}\boldsymbol{e}_x\right]\right)\\&=-\gamma^{-1}\delta^{-1}\partial_y(\pi'_{3/2}\mathbb{F}'_{3/2})\boldsymbol{e}_z=-(\gamma\delta)^{-1}(\partial_y\pi'_{3/2})\mathbb{F}'_{3/2}\boldsymbol{e}_z &\text{(C4)}\\&=\mathbb{F}'_{3/2}\partial_t(\delta\,v'_{3/2})\boldsymbol{e}_z. &\text{(C5)}\end{aligned}$$

Hence, $\overline{\boldsymbol{\nabla}\times(\rho'_{3/2}\partial_t\boldsymbol{u}'_{3/2})}=-\overline{\delta\,v'_{3/2}\,\partial_t\mathbb{F}'_{3/2}}\,\boldsymbol{e}_z$.

C.2. *Using acoustic equations at $O(\epsilon^2)$*

The nonlinear terms $\overline{\boldsymbol{\nabla}\times(\rho'_2\partial_t\boldsymbol{u}'_1)}$ and $\overline{\boldsymbol{\nabla}\times(\rho'_1\partial_t\boldsymbol{u}'_2)}$ require a special analysis but their sum is found to vanish. First, note that $\gamma^{-1}\partial_y$((3.47) + (3.48)) leads, with (3.49), to

$$\partial_y\left(\partial_x u'_2+\partial_y v'_2\right)=-\gamma^{-1}\partial_{ty}\pi'_2=\delta^2\partial_{tt}v'_2, \tag{C6}$$

and, therefore, with the use of (3.47), (3.50) and (C6),

$$\begin{aligned}\overline{\boldsymbol{\nabla}\times(\rho'_2\partial_t\boldsymbol{u}'_1)}&=-\overline{\boldsymbol{\nabla}\times(\boldsymbol{u}'_1\partial_t\rho'_2)}=-\overline{\boldsymbol{\nabla}\times\left[u'_1(\Gamma y\partial_x u'_1-\partial_x u'_2-\partial_y v'_2)\boldsymbol{e}_x\right]}\\&=-\delta^{-1}\partial_y\overline{\left[u'_1(\Gamma y\partial_x u'_1-\partial_x u'_2-\partial_y v'_2)\right]}\boldsymbol{e}_z &\text{(C7)}\\&=-\delta^{-1}\overline{\left[u'_1\Gamma\partial_x u'_1-u'_1\partial_y(\partial_x u'_2+\partial_y v'_2)\right]}\boldsymbol{e}_z\\&=\overline{\Omega'_2\partial_x u'_1}\boldsymbol{e}_z+\delta\overline{u'_1\partial_{tt}v'_2}\boldsymbol{e}_z=\overline{\Omega'_2\partial_x u'_1}\boldsymbol{e}_z-\delta\overline{u'_1v'_2}\boldsymbol{e}_z. &\text{(C8)}\end{aligned}$$

The other nonlinear term can be simplified as well, using successively (3.10), (3.50) and (C8):

$$\begin{aligned}\overline{\boldsymbol{\nabla}\times\left(\rho_1'\partial_t\boldsymbol{u}_2'\right)} &= -\overline{\boldsymbol{\nabla}\times\left(\boldsymbol{u}_2'\partial_t\rho_1'\right)} = \overline{\boldsymbol{\nabla}\times\left(\boldsymbol{u}_2'\partial_x u_1'\right)} = \delta^{-1}\partial_y\overline{\left(u_2'\partial_x u_1'\right)}\boldsymbol{e}_z - \delta\partial_x\overline{\left(v_2'\partial_x u_1'\right)}\boldsymbol{e}_z\\ &= \overline{\left(\delta^{-1}\partial_y u_2' - \delta\partial_x v_2'\right)\partial_x u_1'}\boldsymbol{e}_z - \delta\overline{v_2'\partial_{xx}u_1'}\boldsymbol{e}_z = -\overline{\Omega_2'\partial_x u_1'}\boldsymbol{e}_z + \delta\overline{v_2'u_1'}\boldsymbol{e}_z\\ &= -\overline{\boldsymbol{\nabla}\times\left(\rho_2'\partial_t\boldsymbol{u}_1'\right)}. \end{aligned} \tag{C9}$$

Appendix D. Expression for the leading-order stream function

As detailed in § 3.8, the leading-order streaming flow can be expressed as ($\overline{u}_2 = -\delta^{-1}\partial_y\overline{\psi}_2$, $\overline{v}_2 = \delta^{-1}\partial_x\overline{\psi}_2$), where the stream function $\overline{\psi}_2 = \overline{\psi}_{2H} + \overline{\psi}_{2B} + \overline{\psi}_{2F}$ and

$$\overline{\psi}_{2H} = -\frac{\delta\overline{u}_{slip}}{\sinh(2\delta) - 2\delta}\{(y-1)\sinh(2\delta y) + y\sinh[2\delta(1-y)]\}, \tag{D1}$$

$$\begin{aligned}\overline{\psi}_{2B} = \frac{\mathbb{A}^2\Gamma\mathbb{R}\sin(2x)}{64\delta^3\gamma^2\left[\delta+\cosh(\delta)\sinh(\delta)\right]}&\{-\sinh(2\delta)+\cosh(2\delta y)[2\delta(1-y)+\sinh(2\delta)]\\ &+2\delta y\cosh[2\delta(y-1)] - 2[\delta+\sinh(\delta)^2\sinh(2\delta y)]\},\end{aligned} \tag{D2}$$

$$\begin{aligned}\overline{\psi}_{2F} = \frac{\mathbb{R}\mathbb{F}_{3/2}\mathbb{F}_{3/2}^*\sin(2x)}{32\delta\left[\delta-\cosh(\delta)\sinh(\delta)\right]}&\{\cosh(2\delta y)[2\delta(y-1)+(1-2y)\sinh(2\delta)]\\ &+2\delta y\cosh[2\delta(y-1)] - (2y-1)[2\delta-\sinh(2\delta)-2\sinh(\delta)^2\sinh(2\delta y)]\},\end{aligned} \tag{D3}$$

with $\overline{u}_{slip}$ and $\mathbb{F}_{3/2}$ given in (3.41) and (3.34).

Appendix E. Kinetic energy parameters (K_H, K_F, K_B)

The parameters (K_H, K_F, K_B) defined in (4.3)–(4.5) are given by

$$\begin{aligned}K_H = \frac{\mathbb{A}^4\sinh(\delta)(2(\gamma-1)\sqrt{\mathbb{P}}\sqrt{\mathbb{R}}+3\mathbb{P}+3\mathbb{R})^2}{512\delta\gamma^4(\mathbb{P}+\mathbb{R})^2(\delta-\sinh(\delta)\cosh(\delta))^2}&\\ \{-(8\delta^2+1)\cosh(\delta)+4\delta\sinh(\delta)+\cosh(3\delta)\},&\end{aligned} \tag{E1}$$

$$\begin{aligned}K_F = \frac{\mathbb{A}^4((\gamma-1)\sqrt{\mathbb{R}}+\sqrt{\mathbb{P}})^4}{12288\delta^5\gamma^4\mathbb{P}^2(\delta-\sinh(\delta)\cosh(\delta))^2}&\{108(\delta^3+\delta)\cosh(2\delta)\\ &-3(5\delta^2+7)\sinh(4\delta)+2\delta(\delta^2+18)\cosh(4\delta)+2\delta(8\delta^4+29\delta^2-72)\\ &-2(20\delta^4+111\delta^2-21)\sinh(2\delta)\},\end{aligned} \tag{E2}$$

$$\begin{aligned}K_B = \frac{\mathbb{A}^4\Gamma^2\mathbb{R}^2}{1024\delta^7\gamma^4(2\delta+\sinh(2\delta))^2}&\{2\delta(8\delta^2+9)+2(12\delta^2+5)\sinh(2\delta)\\ &-5\sinh(4\delta)-20\delta\cosh(2\delta)+2\delta\cosh(4\delta)\}.\end{aligned} \tag{E3}$$

References

Aktas, M.K. & Ozgumus, T. 2010 The effects of acoustic streaming on thermal convection in an enclosure with differentially heated horizontal walls. *Intl J. Heat Mass Transfer* **53** (23), 5289–5297.

Bengtsson, M. & Laurell, T. 2004 Ultrasonic agitation in microchannels. *Anal. Bioanal. Chem.* **378** (7), 1716–1721.

Chini, G.P., Malecha, Z. & Dreeben, T.D. 2014 Large-amplitude acoustic streaming. *J. Fluid Mech.* **744**, 329–351.

DARU, V., WEISMAN, C., BALTEAN-CARLÈS, D. & BAILLIET, H. 2021 Acoustically induced thermal effects on Rayleigh streaming. *J. Fluid Mech.* **911**, A7.

HYUN, S., LEE, D.-R. & LOH, B.-G. 2005 Investigation of convective heat transfer augmentation using acoustic streaming generated by ultrasonic vibrations. *Intl J. Heat Mass Transfer* **48** (3), 703–718.

KARLSEN, J.T., AUGUSTSSON, P. & BRUUS, H. 2016 Acoustic force density acting on inhomogeneous fluids in acoustic fields. *Phys. Rev. Lett.* **117**, 114504.

LIGHTHILL, M.J. 1978 Acoustic streaming. *J. Sound Vib.* **61**, 391–418.

LIN, Y. & FAROUK, B. 2008 Heat transfer in a rectangular chamber with differentially heated horizontal walls: effects of a vibrating sidewall. *Intl J. Heat Mass Transfer* **51** (11), 3179–3189.

LOH, B.-G., HYUN, S., RO, P.I. & KLEINSTREUER, C. 2002 Acoustic streaming induced by ultrasonic flexural vibrations and associated enhancement of convective heat transfer. *J. Acoust. Soc. Am.* **111** (2), 875–883.

MASSIH, J.A., MUSHTHAQ, R., MICHEL, G. & CHINI, G.P. 2024 Aspect-ratio-dependent heat transport by baroclinic acoustic streaming. *J. Fluid Mech.* **997**, A7.

MICHEL, G. & CHINI, G.P. 2019 Strong wave–mean-flow coupling in baroclinic acoustic streaming. *J. Fluid Mech.* **858**, 536–564.

MICHEL, G. & GISSINGER, C. 2021 Cooling by baroclinic acoustic streaming. *Phys. Rev. Appl.* **16**, L051003.

NABAVI, M., SIDDIQUI, K. & DARGAHI, J. 2008 Influence of differentially heated horizontal walls on the streaming shape and velocity in a standing wave resonator. *Intl Commun. Heat Mass Transfer* **35** (9), 1061–1064.

QIU, W., JOERGENSEN, J.H., CORATO, E., BRUUS, H. & AUGUSTSSON, P. 2021 Fast microscale acoustic streaming driven by a temperature-gradient-induced nondissipative acoustic body force. *Phys. Rev. Lett.* **127**, 064501.

RAYLEIGH, J.W.S.B. 1896 *The Theory of Sound*, vol. 2, Macmillan.

RAYLEIGH, LORD 1884 I. on the circulation of air observed in Kundt's tubes, and on some allied acoustical problems. *Phil. Trans. R. Soc. Lond.* **175**, 1–21.

RILEY, N. 1997 Acoustic streaming. In *Encyclopedia of Acoustics*, chap. 30, pp. 321–327. John Wiley & Sons. Ltd.

RILEY, N. 2001 Steady streaming. *Annu. Rev. Fluid Mech.* **33** (1), 43–65.

STOCKWALD, K., KAESTLE, H. & ERNST, H. 2014 Highly efficient metal halide HID systems with acoustically stabilized convection. *IEEE Trans. Ind. Applics.* **50**, 94–103,

VAN DYKE, M. 1969 Higher-order boundary-layer theory. *Annu. Rev. Fluid Mech.* **1** (1969), 265–292.